LCLS X-ray mirror measurements using a large aperture visible light interferometer

T. McCarville, R. Soufli, M. Pivovaroff

March 9, 2011

LAWRENCE
LIVERMORE
NATIONAL
LABORATORY

Disclaimer

LCLS X-ray mirror measurements using a large aperture visible light interferometer

Tom McCarville[1], Michael Pivovaroff[1], Regina Soufli[1]

[1]Lawrence Livermore National Laboratory
7000 East Avenue
Livermore, Ca. 94550

Abstract: Synchrotron or FEL X-ray mirrors are required to deliver an X-ray beam from its source to an experiment location, without contributing significantly to wave front distortion. Accurate mirror figure measurements are required prior to installation to meet this intent. This paper describes how a 300 mm aperture phasing interferometer was calibrated to <1 nm absolute accuracy and used to mount and measure 450 mm long flats for the Linear Coherent Light Source (LCLS) at Stanford Linear Accelerator Center. Measuring focus mirrors with an interferometer requires additional calibration, because high fringe density introduces systematic errors from the interferometer's imaging optics. This paper describes how these errors can be measured and corrected. The calibration approaches described here apply equally well to interferometers larger than 300 mm aperture, which are becoming more common in optics laboratories.

I.   Introduction

Optics for the LCLS high energy X-ray beam line, illustrated schematically in Figure 1, deliver the source output to experiment stations. Flat mirrors attenuate incoherent radiation from the source by preferentially reflecting coherent X-rays toward experiments. Experiments may be performed down stream from the flats in the freely expanded beam, or they may be performed were the beam is focused to re-image the source. Focusing is typically accomplished using two elliptical mirrors arranged in a Kirkpatick/Baez configuration.[1]
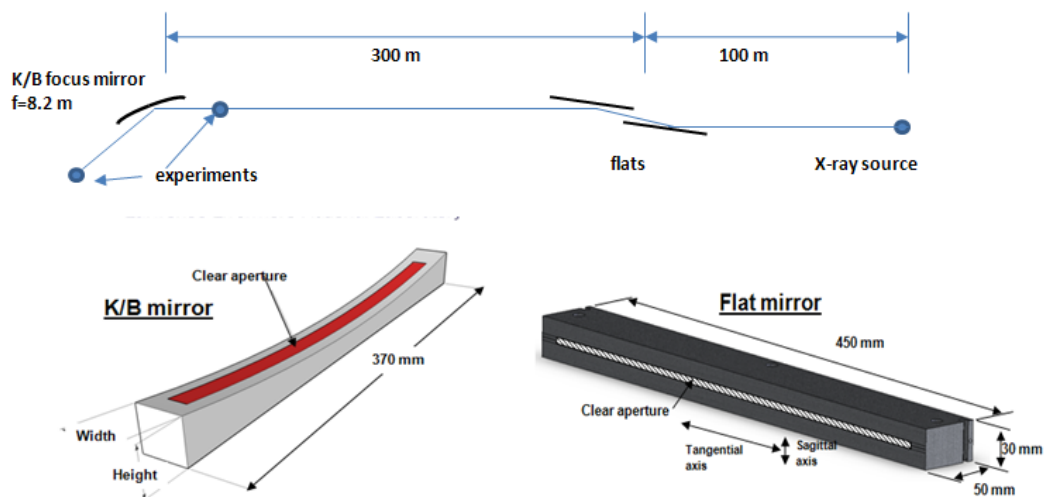

Figure 1. Experiment locations in either the freely expanded beam or at beam focus are illustrated. Typical dimensions of flats and focus mirrors are also shown.

All LCLS mirror substrates are single crystal silicon. The flats are fabricated with about 150 nm of concave spherical curvature (peak to valley). The sphere is reduced by about 10 nm when they are coated with SiC, and the remaining sphere is removed mechanically with the mirror mounted in front of an interferometer. The X-ray beam grazing incidence angle on the flats is 1.3 milli-radians.

A typical K/B focus mirror may have over 3 microns of total curvature, as shown in Figure 2. The dotted line shows the aspheric curvature component required to produce the elliptical shape required to produce an aberration free focus spot. As for flats, the sphere is reduced slightly when the mirror is coated with SiC. The grazing angle for this particular focus mirror is 3.6 milli-radians.
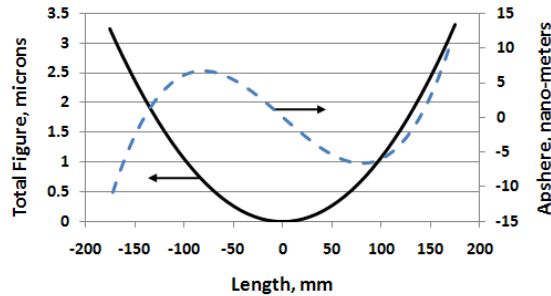

Figure 2. Total curvature specified for a focus mirror is shown as the solid line. The aspheric curvature component obtained by subtracting sphere is also shown as the dotted line.

II.   Figure Tolerances

Sphere

A tolerance for sphere in a flat can be arrived at analytically, because diffraction does not compete significantly with geometric optics as the beam propagates to the focus mirror (ignoring that from the mirror tips). The optical path difference induced in a plane wave incident at grazing angle Θ on a mirror with spherical peak/valley error δ is illustrated in Figure 3. When the beam is re-focused by a focus mirror, the spherical figure error from a flat (or relative spherical errors between the K/B focus mirrors) results in astigmatism. For astigmatism, the normalized peak intensity I (i.e., Strehl ratio) at focus is given by[2],

$$I < 1 - \frac{2\pi^2}{3\lambda^2}(2\delta \sin \Theta)^2 \qquad (1)$$

where λ is the x-ray wave-length. This scaling is plotted as a function of spherical error δ in figure 4 for λ =1 angstrom, at the incidence angles described above for LCLC flats and focus mirrors. The tolerance for spherical error in the focus mirror is lower due to its larger graze angle Θ.
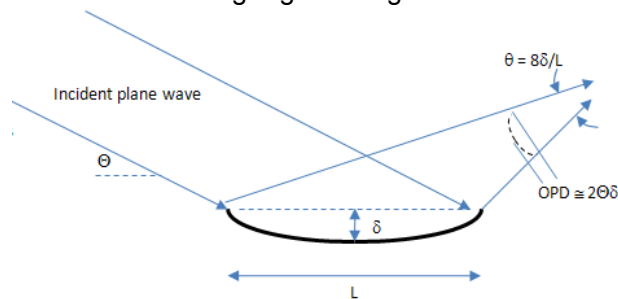

Figure 3. Upon reflection, a spherical figure error with peak/valley δ introduces an optical path difference (OPD) equal to $2\delta\sin\Theta$, and divergence equal to $8\delta/L$.

In principal, a larger tolerance for sphere than that defined by equation (1) can be allowed if the position of one K/B mirror is adjusted relative to the other, converting astigmatism into a focus shift. However, significantly larger tolerances may not be practical if a K/B focus mirror may needs to move by a number of millimeters. An additional constraint is that spherical curvature in a flat produces an elliptical beam upon reflection, affecting clear aperture considerations down stream. The specification for sphere in LCLS flats was set at 10 nm (peak to valley) after mounting to limit the change in beam radius to <10% upon reflection.
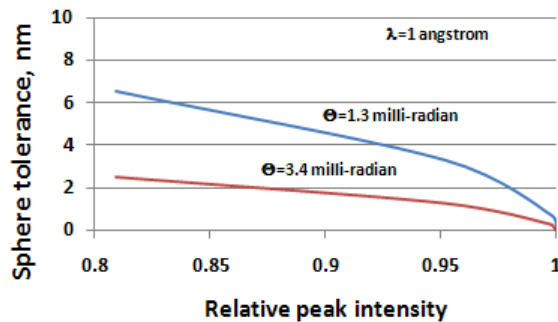

Figure 4. The tolerance for sphere calculated using equation (1).

A-sphere in Flats

A figure error of length scale L in a flat initiates a phase disturbance with length scale $L*\sin\Theta$ in the reflected beam, where Θ is the graze angle. The transverse dimensions of the phase disturbance increase with distance z from the mirror as $L*\sin\Theta*(1+(z/Ra)^2)^{1/2}$, where the Rayleigh length $Ra=\pi*(L*\sin\Theta)^2/(4\lambda)$.[3] Ray optics apply for distances z << Ra, diffraction dominates when z >>Ra.

The Rayleigh length is plotted as a function of figure error scale length in Figure 5, for 0.1 nm wave length, and 1.3 milli-radian mirror graze angle. By comparing the Rayleigh length to the 200 m distance from the flats to the focus mirror, it is apparent figure errors with L < 1 mm diffract light well beyond the focus mirror acceptance aperture. These errors result in a loss of beam power, without significantly changing the intensity profile. The specification for LCLS flats is < 0.5 nm rms for this scale length, to limit the power loss to < 1%.

For figure error length scales > 25 mm, the phase and intensity do not evolve significantly along the propagation path from the flat to the focus mirror. A Gaussian intensity profile from the source would remain Gaussian, up to the focus mirror, with a reduction in transverse coherence length.

Between these two length scale extremes, the phase and intensity evolves in a manner not readily characterized by simple rules. Numerical solution of the Fresnel equation is required to predict the phase and intensity distribution along the path to the focus mirror. If the figure errors are large enough, the intensity that arrives at the focus mirror can be highly modulated.
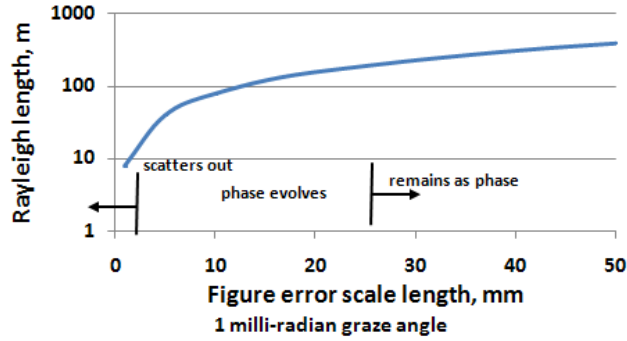
Figure 5. Rayleigh range vs. figure error scale length for 1 angstrom wavelength.

While mirror reflections introduce a wide range of phase error length scales, with different implications on how phase and intensity evolve, re-imaging the source faithfully at a focus still requires that some form of the Rayleigh quarter wave rule apply. The Marechal criterion describes how the peak intensity I at focus is reduced as a function of rms figure error.[2] Expressed in terms of the mirror graze angle Θ and rms figure tolerance δ_{rms} , this criterion is

$$ I \ < 1 - \left(\frac{2\pi}{\lambda}\right)^2 (2\delta_{rms} \sin \Theta)^2 \qquad . \qquad (2) $$

Equation (2) is plotted in Figure 6 for LCLS flats with 1.3 milli-radian graze angle. The LCLS flats are specified to have < 2 nm rms a-sphere figure error for spatial scales from 1 mm up to full mirror length. As shown in Figure 6, reflection off two flats reduces the normalized peak intensity to about 0.8 with this specification.
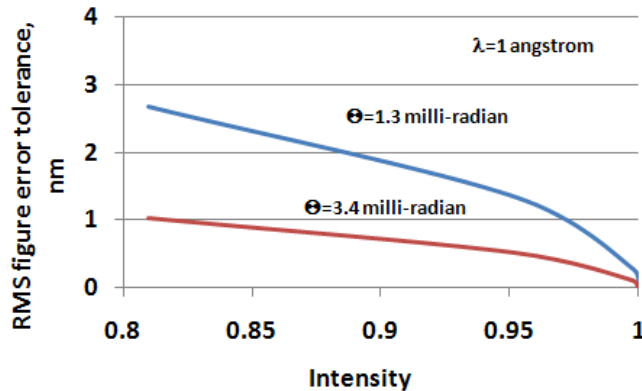

Figure 6. RMS figure error vs. rms intensity for the graze angles of LCLS flats and focus mirror.

A-sphere in Focus Mirrors

The a-sphere tolerance for focus mirrors is simpler to contemplate because at beam focus, all phase disturbances produced by mirror reflections are in the far field. In the far field, the Fraunhofer approximation describes the effect of focus mirror figure errors. The modulated intensity and phase propagated from the flats to the focus mirror, plus the focus mirror figure errors, is the input for the calculation. Examples of detailed calculations using measured figure error data are contained in the references.[4,5]

Because focus mirrors are generally used at larger graze angles than flats, measuring and maintaining focus mirror figure is a more difficult challenge. Figure 6

shows the Marechal criterion for an LCLS K/B focus mirror used at 3.4 milli-radians. A-sphere figure errors < 1 nm rms are required to maintain Strehl > 0.8 nm.

III.   Interferometer Calibration

A visible light phasing interferometer is capable of measuring figure accurate to < 1 nm.[5] Absolute calibration of a reference flat was performed to reach that goal, and is described below.

The three configurations required to calibrate a transmission flat along a horizontal axis are shown in Figure (7).[6] Two transmission flats mountable onto the interferometer and labelled T1 and T2, are required. A third flat that can rotate 180° about its optic axis, labelled R, is also required. Particular care must be taken to mount flat R so that its figure does not change significantly when the gravity load is reversed.

The interferometers fixed coordinate system is shown as solid lines in the left hand side of Figure 7, and local coordinates attached to each optic as dotted lines. All the local coordinates are fixed by the first two measurements, labelled F1 and F2. For the third measurement, F3, the optics local x coordinates are both opposite in sign to the interferometer coordinate. Reversing the x coordinates of the data taken from this third measurement allows a solution for figure T1, T2, and R.

$$F1(x) = T1(x) + T2(x) \qquad F2(x) = T1(x) + R(x) \qquad F3(x) = T2(-x) + R(-x)$$

• To solve for T1(x), T2(x), R(x), convert T2(-x) to T2(x), R(-x) to R(x)

$$T1(x)=1/2[F1(x)+F2(x)-F3(-x)] \qquad T2(x)=1/2[F1(x)-F2(x)+F3(-x)] \qquad R(x)=1/2[-F1(x)+F2(x)+F3(-x)]$$
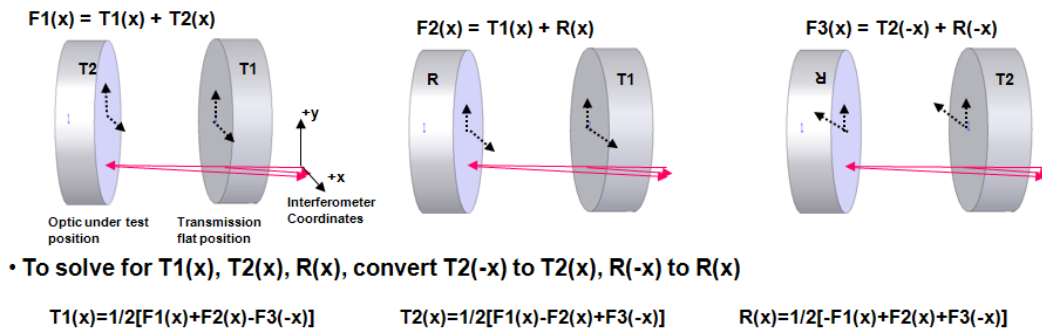
Figure 7. Geometry for calibrating transmission flats along the horizontal axis.

Two additional independent measurements that can be made are shown in Figure 8. These configurations cannot be used to solve for figure, because the local coordinates have opposing sign. But the two configurations are useful for testing the accuracy of the solution obtained from the geometry in Figure 7. Measurements F4 and F5 are shown in Figure 8, along with a sample of the calibration error term that can be evaluated from the data.

$$F4(x) = T1(x) + R(-x)+Error(-x) \qquad F5(x) = T2(-x) + R(x)+Error(x)$$

Error check
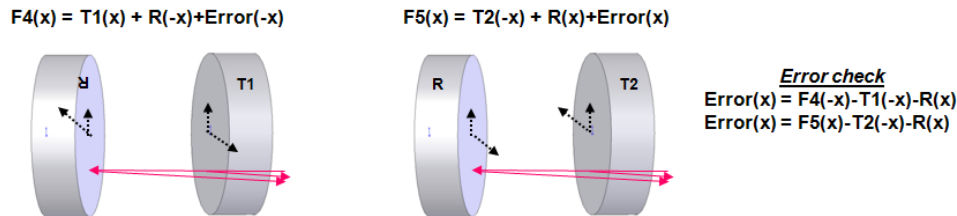Error(x) = F4(-x)-T1(-x)-R(x)
Error(x) = F5(x)-T2(-x)-R(x)

Figure 8. Configurations used to sample transmission flat calibration error.

The figure measured from a three flat test is shown on the left in Figure 9. Flat T2 was used to measure LCLS mirrors. The calibration error, sampled using the additional two geometries shown in Figure 8, is shown on the right in Figure 9. These measurements indicate the calibration error (sphere plus a-sphere) is about 1 nm

peak to valley, with an rms error <0.5 nm. It remains to be seen if this can be further improved, or if this is the fundamental limit of the interferometer hardware.
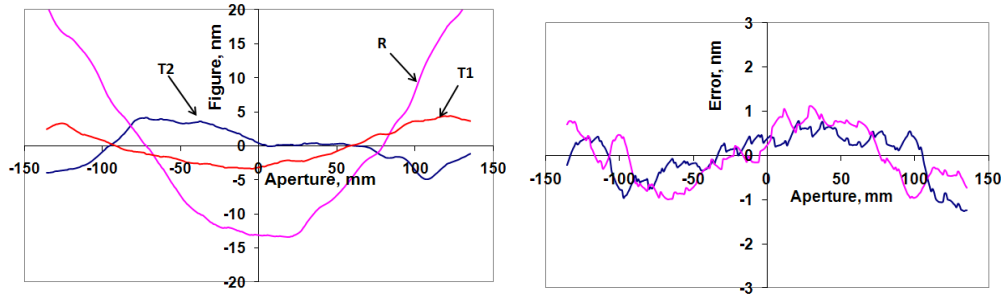

Figure 9. Three flat calibration results are shown on the left. The measured error using the other two independent geometries that are available is shown on the right.

IV.   Measuring LCLS Flats

Four 450 mm flats for LCLS, fabricated by Zeiss, have been measured on the calibrated interferometer. Because the interferometer aperture is limited to 300 mm, three measurement files are stitched together with about 60% data point overlap. Because the overlap is large and measurement errors are small, a number of simple overlap algorithms work equally well.

All four met the specification for < 2 nm rms a-sphere, both when they were received and after mounting. The best flat received is shown in Figure 10. The total figure is plotted on the left hand side, and the a-sphere component of the total on the right. The a-sphere plot contains two data sets: one measured by these authors, and a data set measured independently at Zeiss. The agreement demonstrates flats can be accurately measured to < 2 nm rms a-sphere. It also indicates flats fabricated to better than 1 nm rms are within near reach.
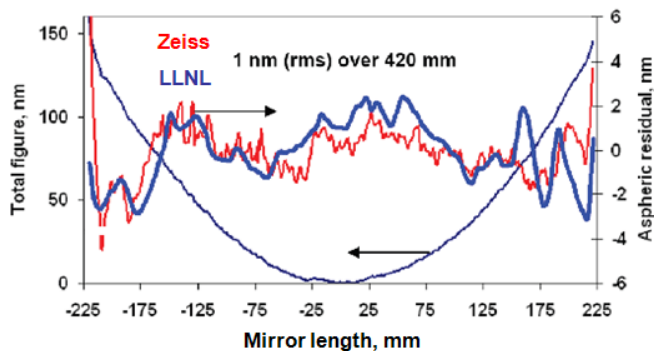

Figure 10. Total figure for one of five LCLS mirrors before it was mounted and sphere removed. There are two data sets for a-sphere: one measured by these authors, and another measured independently by Zeiss.

The flats are fabricated with about 150 nm of concave sphere. The spherical curvature is reduced by about 10 nm when the mirror is coated with SiC, with no measureable increase in a-sphere. The remaining sphere is reduced to < +/- 10 nm using a mechanical bender designed into the mount, while observing the mirror with the interferometer. The mounting, measuring, and bending process takes less than four hours to complete. The total figure after a mirror was coated and bent nominally flat is compared to the as-received figure on the left hand side of Figure 11. When sphere is subtracted from these three plots, shown on the right of Figure 11, the change in a-sphere is barely measurable.
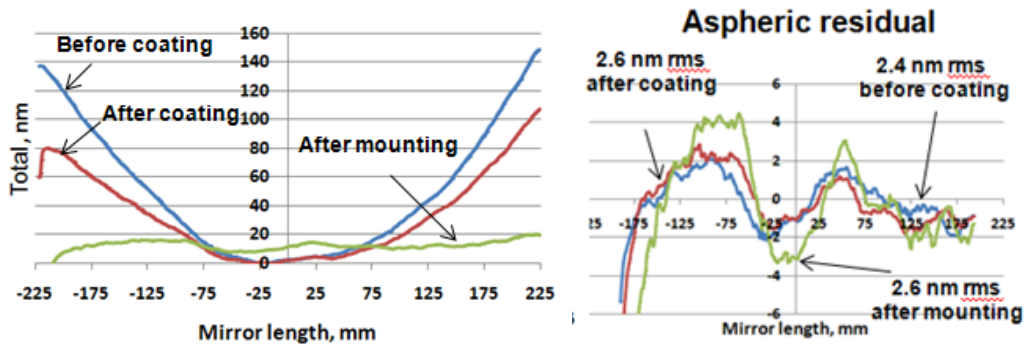
Figure 11. Total figure of a flat as received, after coating, and when mounted and bent nominally flat in front of an interferometer is shown on the left. The a-sphere component for each case is shown on the right.

V.   Measuring Focus Mirrors

There are a number of possible configurations for measuring a focus mirror with an interferometer. Errors introduced by interference cavity path length are minimized when the focus mirror is as close as possible to the refection flat, as shown in Figure 11. This configuration results in high fringe density across the aperture, and limits the maximum curvature that can be measured. For a 512 pixel camera, and three pixels per fringe, the peak/valley that can be measured using a HeNe laser is limited to about 12 microns. This range is adequate to measure many X-ray focus mirrors of interest.

High fringe density introduces an additional error source.[6] Rays reflected from the curved parts of the focus mirror take a substantially different path back to the detector from those reflected off the transmission flat, as illustrated in Figure 11. The difference is small at the interferometers large optics, but significant at the small imaging optics near the CCD. If rays passing through the imaging optics were deflected in exact linear proportion with the distance to the optic axis, these different ray paths would not introduce a measurement error. But in practice, some path dependent error is introduced as fringe density increases.

Figure 11. Configuration for measuring focus mirrors with minimum interference cavity path length and calibrated optics.

This fringe dependent measurement error is easily quantified by observing a nominally flat mirror at null fringe density, and then incrementally tilting it. The interferometer will report false curvature as tilt is increased and fringes accumulate. This erroneous report of figure change in the test flat can be recorded as a function of tilt angle at every point across the aperture, and converted into a systematic correction that can be applied when measuring focus mirrors.

The correction that would be applied to the focus mirror in Figure 2, measured for the 300 mm interferometer used to measure LCLS flats, is shown in Figure 12. As

expected the correction passes through zero at aperture center, where the focus mirror slope would be zero. The shape of the correction away from the center suggests coma is introduced by the imaging optics away from the mirror center as fringes accumulate. The asymmetry on the right of the curve suggests the imaging optics alignment is not quite optimal. While the correction is quite small compared to the mirror's total curvature, it is significant compared to the a-sphere curvature that is intended for this mirror (see Figure 2).
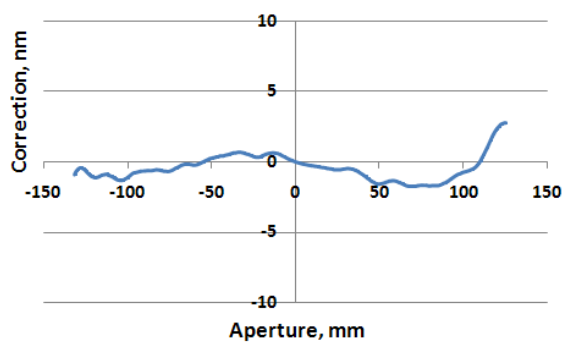

Figure 12. Correction that would be applied to measured data for the center +/- 140 mm of the focus mirror shown in Figure 2.

VI. Conclusions

The objective of this effort was to install LCLS flats with < 10 nm of spherical curvature, and < 2 nm rms a-sphere. The objective was met by measuring the mirrors after fabrication, coating and mounting, using a 300 mm aperture phasing interferometer calibrated to an accuracy < 1 nm. The key to calibrating the interferometer accurately was to sample the error using independent geometries that are available. The results of those measurements helped identify and reduce calibration error sources.

The approach used to measure flats applies equally well to focus mirrors, provided an additional calibration is performed to measure the error introduced by fringe density. This calibration has been performed on the 300 mm aperture interferometer, and the measurement correction was evaluated for a typical focus mirror.

The 300 mm aperture limitation requires stitching figure measurements together for many X-ray mirrors of interest, introducing another possible error source. Stitching is eliminated by applying the calibrations described above to larger aperture instruments. The authors are presently extending this work to a 600 mm instrument. Instruments with 900 mm aperture are now becoming available, which would accommodate the largest mirrors of interest.

References
(1) P. Kirkpatrick and A. V. Baez, "Formation of optical images by x-rays" J. Opt. Soc. Am. 38, 776-774 (1948).

(2) M. Born & E. Wolf, <u>Priciples of Optics</u>, Pergamon Press, Chapter IX.
(3) R. Guenther, <u>Modern Optics</u>, Wiley & Sons, 1990, p. 336.
(4) L. Samoylova, H. Sinn, F. Siewert, H. Mimura, K. Yamauchi, T. Tschentsdcher, Requirements on hard X-ray Grazing Incidence Optics for European XFEL: Analysis and Simulation of Wavefront Transformations, Proc. Of SPIE Vol. 7360, 73600E
(5) A. Barty, R. Soufli, T. McCarville, S. Baker, M. Pivovaroff, P. Stefan, R. Bionta, Predicting the coherent X-ray wavefront focal properties at the Linac Coherent Light Source (LCLS) X-ray free electron laser, 31 Aug. 2009, Vol. 17, No. 18, Optics Express 15508.
(6) Progress in Optics, ed. E. Wolf, Vol. XIII, 1976, p. 118.
(7) D. Phillion, General Methods for Generating Phase Shifting Interferometry Algorithms, Applied Optics, Vol. 36, No. 31, Nov. 1997.

Email corresponding author: mccarville1@llnl.gov   Preference: Oral